Storm mergers. Part I: Preliminary numerical investigations of merger events.

Ryan M. Hastings * and Yvette P. Richardson

The Pennsylvania State University, University Park, Pennsylvania

1. Introduction

The role of storm interactions and mergers in tornadogenesis and subsequent storm evolution has received some attention in the literature, although it remains a largely unexamined problem. A few observational studies have been carried out on tornadoes associated with mergers between supercells (e.g. Wurman et al. 2007), and Finley et al. (2002) used nested grids in a numerical investigation of tornadogenesis associated with mergers in an HP supercell. The significance of these incidences is highlighted by Lee et al. (2006), who found a statistically significant correlation between tornadogenesis supercell merger during an outbreak on 19 April 1996 in Illinois. Approximately 55% (20 out of 37) of the tornadoes began within five minutes of a merger, and 57% of the supercell mergers were associated with tornadoes. However, not every merger results in a tornado. The question of what the outcome of a merger will be is thus of importance to the operational community.

Mergers between convective clouds have been studied for some time [see Westcott (1984) for a review]. Most of these studies have involved subtropical and tropical systems. It has been long established that when these systems result from mergers, they are taller, larger, more persistent, and produce more precipitation than isolated systems. For these non-rotating systems, some understanding of the conditions favoring and the dynamics governing mergers has been established. Cloud mergers require a horizontal pressure gradient to force them together, which is commonly found when neighboring clouds are of different size or age (Orville et al. 1980, Turpeinen 1982), and is often associated with an area of increased convergence between the outflows of the systems (Tao and Simpson 1989). Mergers may be associated with differential cell motion, and can involve the growth of new cloud between the older cells (i.e.,"cloud bridge") or simply the expansion of one cloud to envelope another (Westcott 1994). Some of these mechanisms have been observed in supercells. For example, Lee et al. (2006) found that two common modes for supercell merger involved the development of cloud bridges or the initiation of a new cell at the location where two storm tracks intersect. The role of convergence along gust fronts, with associated vertical motion, and subsequent tilting and stretching of vorticity, has been noted by Lee et al. (2006), Finley et al. (2002) and was hypothesized to play a role in tornadogenesis by Wurman et al. 2007.

A variety of definitions for cloud merger have been used in the literature (Westcott 1984). These have included definitions based on cloud water mixing ratio, radar reflectivity, and dynamic criteria such as the joining together of two updrafts. Because this work is intended ultimately to be of service to the operational community, the primary definition for a merger will be based on radar reflectivity. We will consider two cells as having merged if an arbitrarily defined contour of high reflectivity is continuou across them and only one maximum remains. This will subsequently be referred to as an "echo merger." As we are also interested in the dynamics, we will also pay attention to updraft mergers, although this will be secondary when defining whether or not a merger has occurred.

This work comprises two main components: Numerical studies of idealized supercell mergers, and observational studies of actual merger events, with the goal of identifying the dynamical processes at work in determining the course and outcome of these events. In this paper, the preliminary numerical investigations will be discussed. A subsequent paper (Hastings et al. 2010) takes an initial look at the most well sampled merger from VORTEX2.

2. Methods

In order to investigate the dynamics involved in supercell mergers, a set of idealized numerical simulations is carried out. The experimental design is partly an exploration of a range of cell interactions, together with more targeted simulations designed such that idealized storm paths (i.e., the paths they would take were it not for their interaction) should result in a merger event. This reasoning will be briefly outlined, followed by a more detailed description of the experiments.

Differential motion of the storms is an almost *a priori* requirement for a merger. It is well known that supercell motion is dependent on the stage of the storm's evolution (Klemp 1987) when the environment is characterized by a straight hodograph. In the initial stages, when the storm is an ordinary cell that has not developed significant

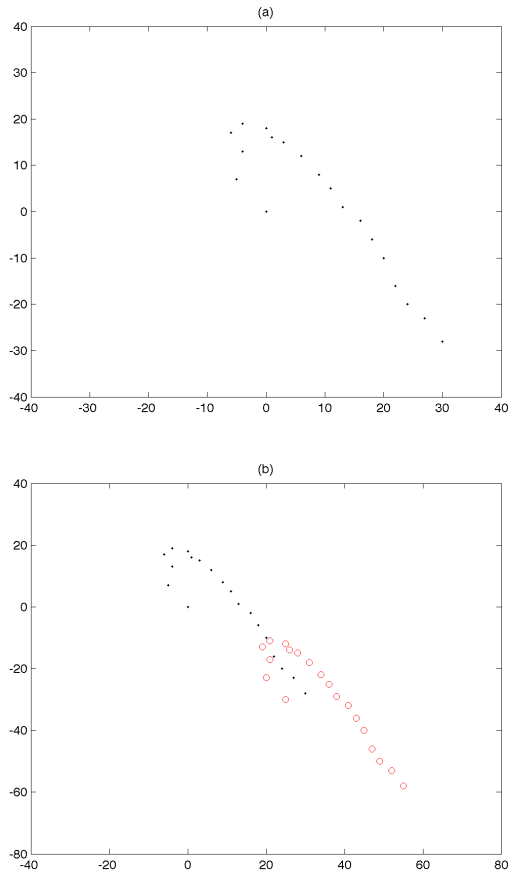

FIG. 1. Example of storm tracks for planning target runs. (a) Location of maximum updraft after every ten minutes for a single supercell. (b) Superposition of second identical track with location shifted.

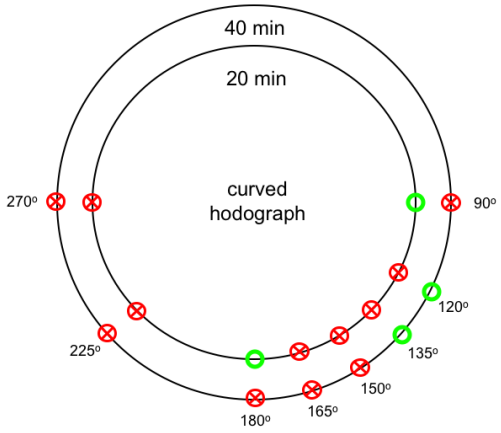

FIG. 2. Summary of results from semicircle hodograph ring runs. Green circles represent successful mergers, red circles with crosses indicate no mergers occurred. Position around the ring indicates the compass angle at which the second bubble was initiated. The inner ring represents the bubbles initiated at 20 minutes, the outer at 40 minutes.

dynamic perturbation gradients on the flanks, the motion is roughly the same as the mean wind over the 0–6 km layer. As the storm develops rotation, lifting pressure gradients associated with the maximum vorticity magnitude at mid-levels on the storm flanks resulting from the interaction of the storm updraft with the environment cause the propagation of the supercell away from the mean wind. This is accompanied by storm splitting, which results in a left-mover dominated by anticyclonic vorticity and a right-mover dominated by cyclonic vorticity. In environments with sufficient curvature in the hodographs, the left-mover is suppressed and the right-mover is favored owing to the linear perturbation pressure pattern caused by the interaction of the updraft with environmental shear.

Thus, some conditions making supercell merger possible can be elucidated. The two most likely scenarios involve the interaction between a left- and a right-mover, and between a supercell whose motion deviates from the

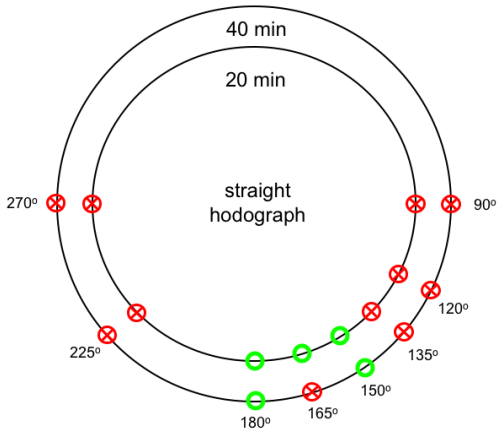

FIG. 3. As Figure 2, but for the unidirectional hodograph.

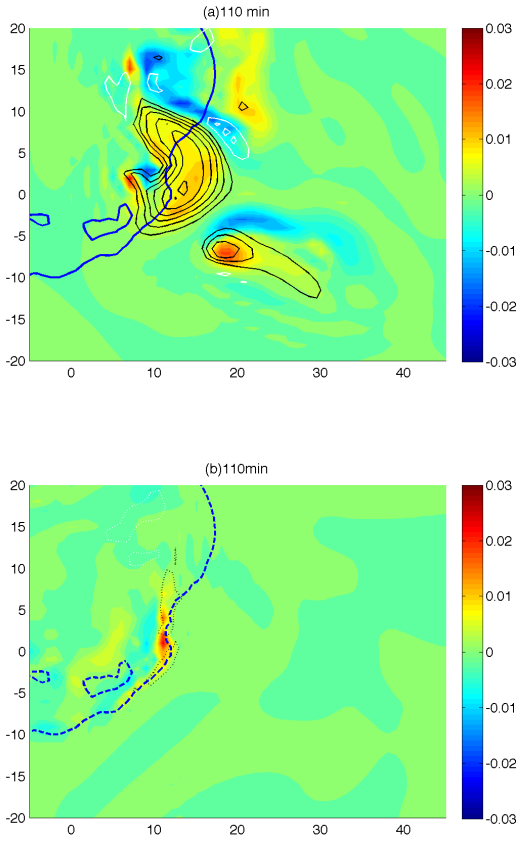

FIG. 4. (a) Vorticity (colored) and vertical velocity at 100 minutes at 4.21 km AGL for M35 run. Positive (negative) vertical velocities are contoured in black (white) every 5 m s^{-1}. The blue line is the -1 perturbation in potential temperature at 100 m AGL. (b) Vorticity (colored) at 100 m AGL for the same run. The blue line is the -1 potential temperature perturbation. 0.01 s^{-1} convergence is contoured with a dotted black line.

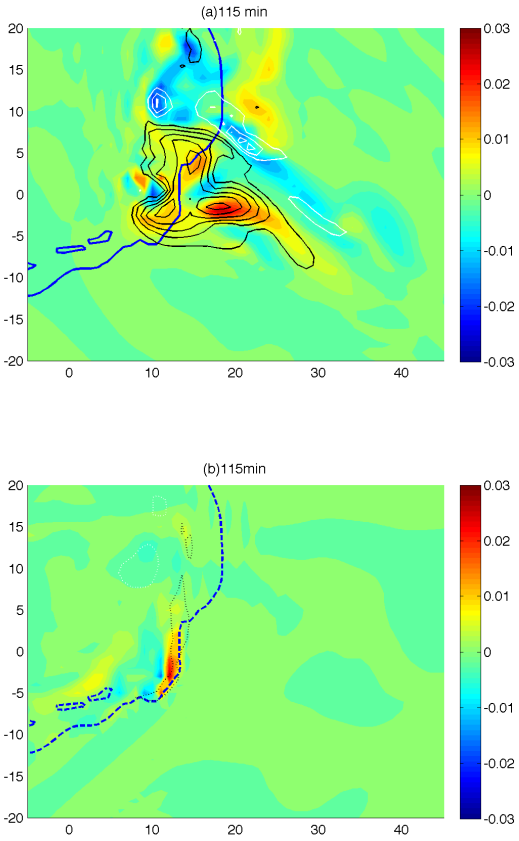

FIG. 5. As Fig 4 at 115 minutes.

mean flow merging with a cell that has not yet matured and turned.

Previous attempts to investigate storm interactions have involved initializing cloud models with two thermal perturbations in an environment known to produce supercells in models, with subsequent interactions between left- and right-movers (e.g., Bluestein and Weisman 2000, Jewett et al. 2008). Because of the potential importance of having the storms encounter one another when they are at different points in their life cycle, these idealized experiments involve introducing a second thermal bubble at a predetermined time and location near the original perturbation. In these experiments, the second perturbation is identical to the first in size and strength.

The cloud model CM1 is initialized under typical conditions for producing a supercell. The base thermodynamic state is defined with the analytic sounding from Weisman and Klemp (1982), with a potential temperature perturbation that is 2 K at its maximum and has a horizontal (vertical) radius of 10 km (1.5 km) and is centered 1.5 km AGL. The perturbation follows a cosine squared function. The grid is 200 km x 200 km x 20.4 km. Horizontal grid spacing is 1km x 1km, and the vertical levels are stretched from 200 m at the ground to 800 m at 10 km AGL, and above that are uniform. Grid motion is adjusted to keep the storms near the center, though they are allowed some slight forward motion. The lateral boundary conditions are open, with a Rayleigh sponge layer above 14 km. No surface physics or radiation are specified. The microphysics are governed by the NASA-Goddard LFO scheme.

The first set of runs, hereafter called *ring runs*, introduce the second bubble at a point 30 km from the origin, at compass directions 90°, 120°, 135°, 150°, 165°, 180° 225° and 270°. Two different hodographs are employed. The unidirectional runs use the wind profiles from Weis-

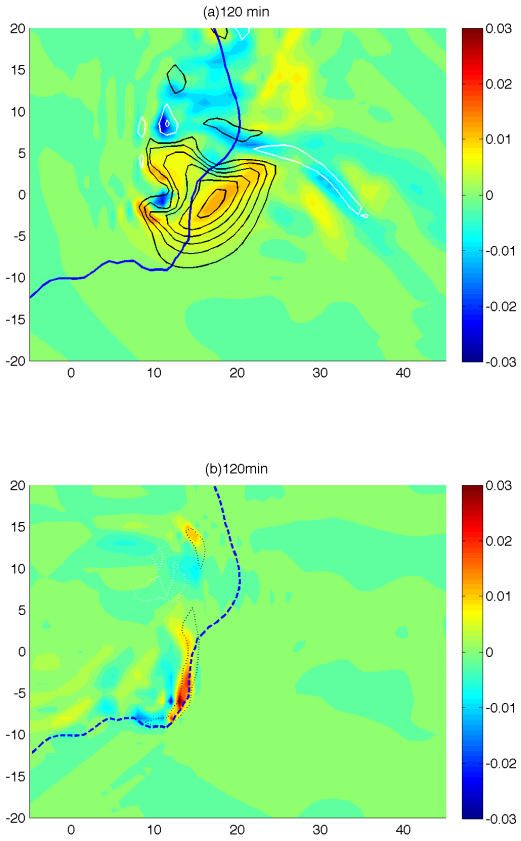

FIG. 6. As Fig 4 at 120 minutes.

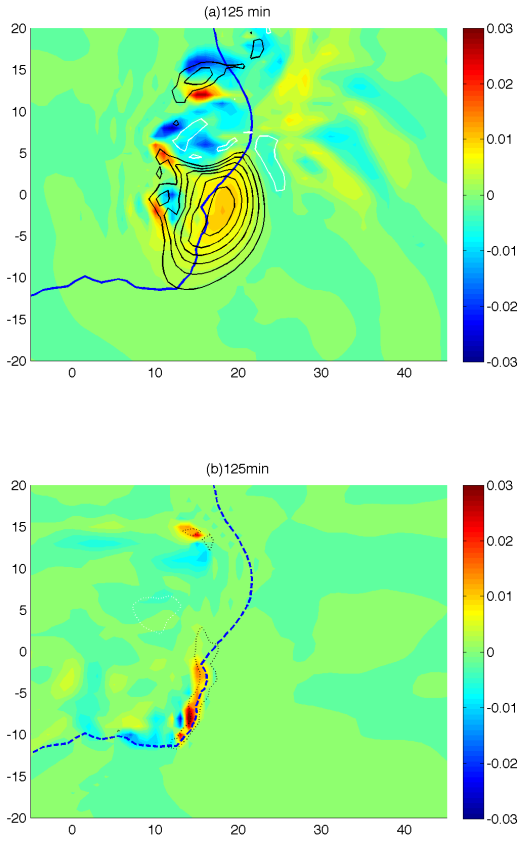

FIG. 7. As Fig 4 at 125 minutes.

man and Klemp (1982) with

$$u = 35\text{m s}^{-1} \tanh(z/3\text{km}) \quad (1)$$

$$v = 0. \quad (2)$$

The curved runs use the semicircular wind profiles described in Weisman and Klemp (1984) with a diameter of 35 m s^{-1}. The second bubbles are introduced at 20 minutes and 40 minutes.

The second set of runs, hereafter called *target runs*, attempt a more careful approach to exploring the timing of the process. With the known storm track of a control run with a single storm (Fig. 1), the location of the second identical thermal perturbation can be selected to give an anticipated merger at a specific point in the life cycle of the supercell. Because interactions between left- and right-movers have previously been studied, this set of runs is only concerned with interactions involving a right-mover and an immature or maturing supercell. Thus the semicircular hodograph is used.

3. Results

Several successful mergers resulted from this suite of experiments. From the ring runs, sensitivity to both timing and original bubble location could be seen. Of the four target runs attempted, only two had mergers owing to the suppression of the second cell in the vicinity of the mature supercell in the non-merger runs.

a. Ring runs

Figures 2 and 3 summarize the results of the ring runs. For the curved hodograph, the primary type of merger is between a mature right-mover and a less mature one. The success is clearly sensitive to the timing of the initiation of the second bubble. The only type of merger for the straight hodographs is between left- and right-movers. This is also the type of merger that occurred with the run with the 180° curved run (Fig 2).

Two main modes of failure for merger can be seen from these runs. For those bubbles initiated on the eastern half of the ring, the interactions tend to result in quasi-linear convective systems with embedded mesocyclones.

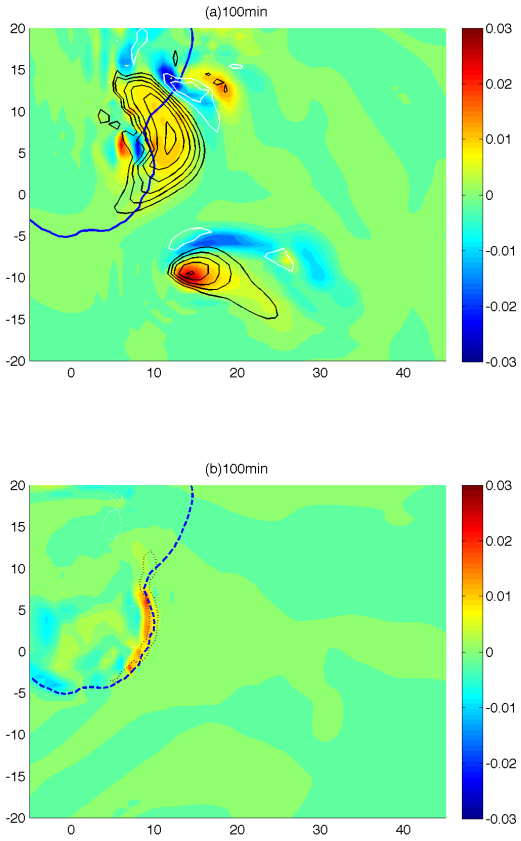

FIG. 8. (a) Vorticity (colored) and vertical velocity at 100 minutes at 4.21 km AGL for M40 run. Positive (negative) vertical velocities are contoured in black (white) every 5 m s^{-1}. The blue line is the -1 perturbation in potential temperature at 100 m AGL. (b) Vorticity (colored) at 100 m AGL for the same run. The blue line is the -1 potential temperature perturbation. 0.01 s^{-1} convergence is contoured with a dotted black line.

For those on the western half, the new cells soon get surrounded by the cold pool of the original supercell and subsequently weaken.

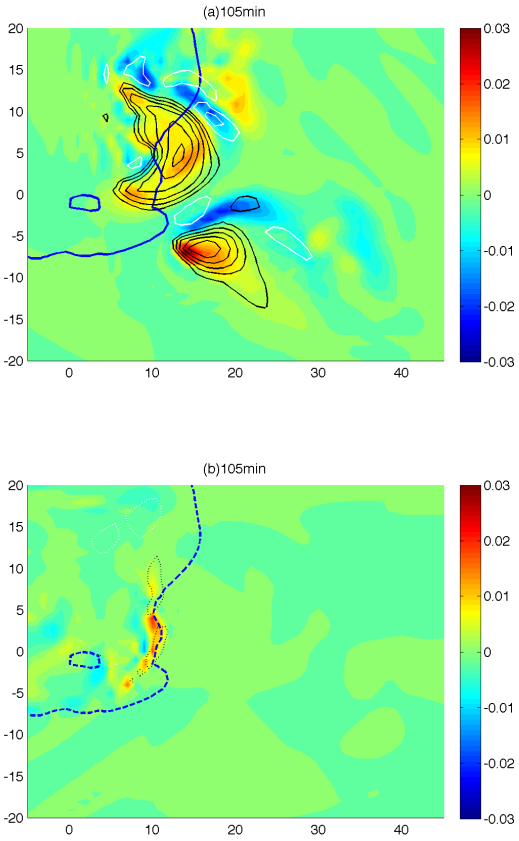

FIG. 9. As Fig 8 at 105 minutes.

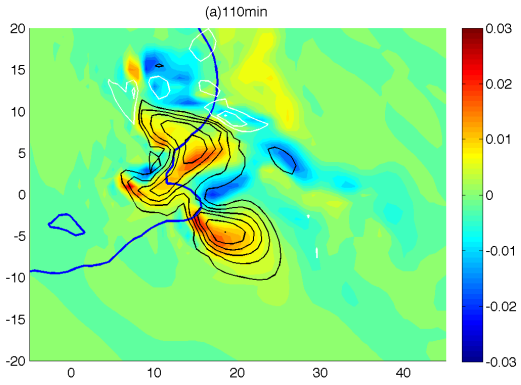

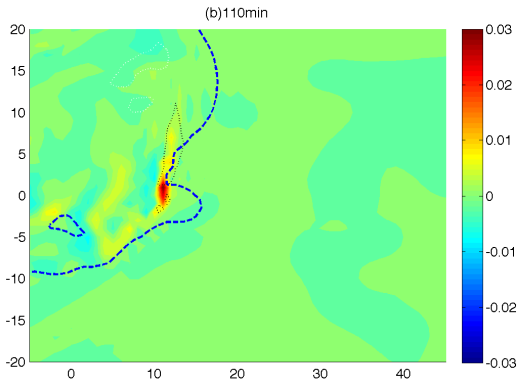

FIG. 10. As Fig 8 at 110 minutes.

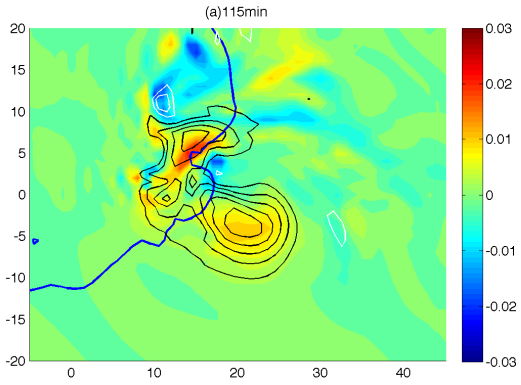

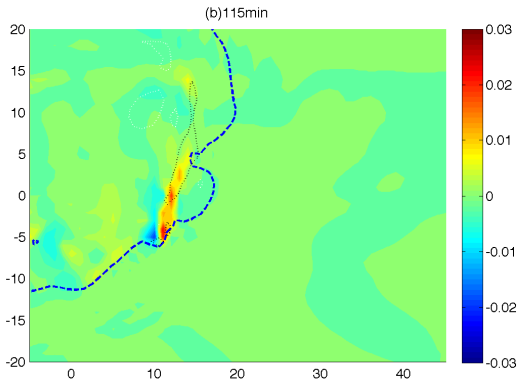

FIG. 11. As Fig 8 at 115 minutes.

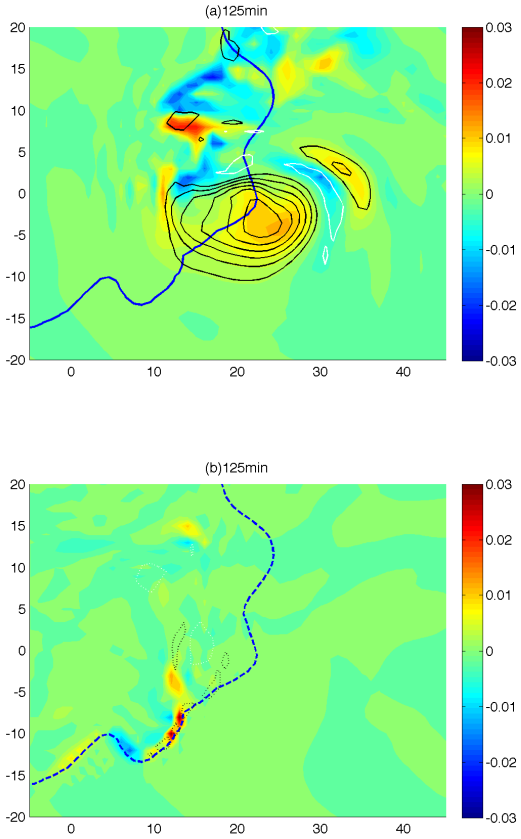

FIG. 12. As Fig 8 at 125 minutes.

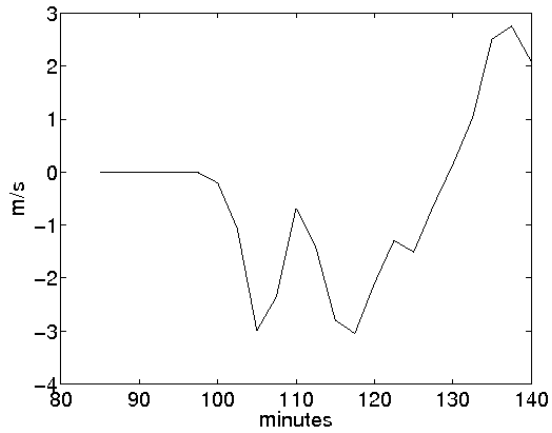

FIG. 13. Difference between maximum vertical velocity between the M35 run and a control (isolated) supercell, in the domain pictured in Figs 8–12 in the 0–6 km layer. Positive (negative) values indicate higher vertical velocity maxima in the merging (control) cell.

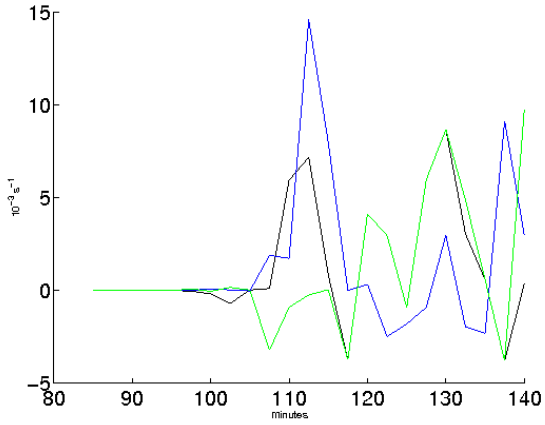

FIG. 14. Difference in maximum vertical vorticity between the M35 and a control (isolated) supercell, in the domain pictured in Figs 8–12. Green is at 100 m AGL, blue at 4.21 km AGL, and black over the entire 0–6 km layer. Positive (negative) values indicate higher vertical vorticity maxima in the merging (control) cell.

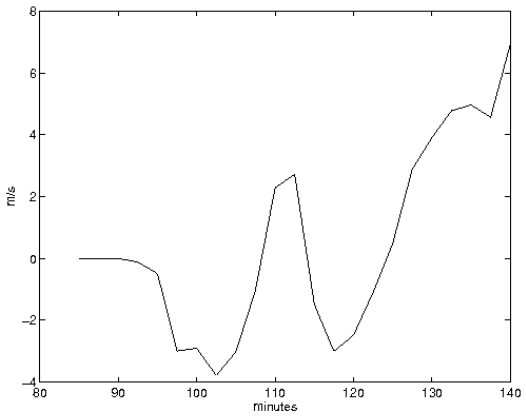

FIG. 15. Difference between maximum vertical velocity between the M40 run and a control (isolated) supercell, in the domain pictured in Figs 8–12 in the 0–6 km layer. Positive (negative) values indicate higher vertical velocity maxima in the merging (control) cell.

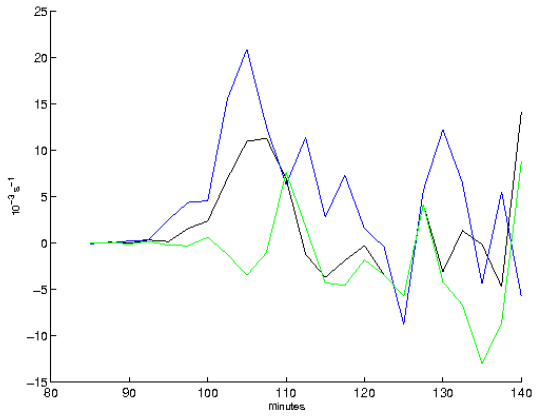

FIG. 16. Difference in maximum vertical vorticity between the M40 run and a control (isolated) supercell, in the domain pictured in Figs 8–12. Green is at 100 m AGL, blue at 4.21 km AGL, and black over the entire 0–6 km layer. Positive (negative) values indicate higher vertical vorticity maxima in the merging (control) cell.

b. Target runs

As previously mentioned, only two of the target runs involved supercell mergers. These are the runs in which the second perturbation has been allowed to mature for 35 and 40 minutes minutes (hereafter referred to as M35 and M40). Figures 4–12 illustrate the process for both supercells.

In both cases, final result is a strong supercell. However, both the vertical vorticity and vertical velocities are significantly stronger in both M40 and M35 than in the control run. Furthermore, M40, with an extra five minutes to mature, is significantly stronger than M35 (Figs 13–16). At 240 minutes, M40 has a maximum vertical velocity below 6 km that is more than 6 m s^{-1} stronger than the control run (Fig. 15), while M35 does not even reach 3 m s^{-1} in magnitude above the control. A similar pattern can be seen in the vertical vorticity at 4.21 km AGL, although the vertical vorticity at 100 m is comparable for both cases (Fig. 14 and 16). The maximum vertical vorticity seems to surge just as the merger begins for both cases. The vertical velocity, on the other hand, is suppressed for a few minutes before and after the event.

A striking difference between the mergers is evident by considering the velocity and vorticity structures at these levels. The developing updraft in M35 readily joins with the original cell. As it approaches, the 25 m s^{-1} updraft contour at the 4.21 km AGL of the original cell splits into two separate maxima, while the third cell strengthens to greater than 30 m s^{-1}. All three of these updraft maxima are contained with the 20 m s^{-1} contour (Fig. 5(a)). Five minutes later, only the new updraft remains (Fig. 6(a)). It is worth noting that in M35, the new cell has not yet developed a cold pool. Some anticyclonic vorticity develops between the updraft maxima at 115 minutes (Fig. 5(a)), but it quickly weakens, coincident with the weakening of the mesocyclone. Near ground level, the line of vertical vorticity along the gust front intensifies, with the maximum vorticity shifting to the south, and is not seriously disrupted (Figs 4(b)–7(b)).

In contrast for M40, the new storm is beginning to develop a cold pool and is in the process of splitting. Its approach is more disruptive to the original updraft (Fig. 11(a)). Indeed, from a kinematic standpoint, instead of merging, this interaction is more like updraft replacement, as the maximum of the new cell retains its integrity while that of the original cell dissipates. The anticyclonic maximum remains outside the 5 m s^{-1} contour. Near the surface, the original line of vorticity is disrupted, but is quickly replaced by new vorticity maxima just south of the updraft (Figs. 8(b)–12(b)).

4. Conclusions

A series of model experiments were designed to move towards exploring the dynamics of storm mergers. Some sensitivity to secondary storm location is revealed, although the results suggest that the relative maturity of the merging storm may play a more significant role in determining the outcome of the merger. In the target runs, a difference of five minutes in the secondary storm lifetime was enough to yield significant differences in the vertical velocities, the mid-level vertical vorticity, and the overall process of the merger.

The next question to explore is the dynamical causes for the observed changes in storm structure during the merger. Thus, the next step is to perform Lagrangian calculations along parcel trajectories through the areas of interest.

Finally, it is worth taking a moment to review the two definitions of merger mentioned in the introduction. The initial look at these model runs suggests a strong correlation between those two types of mergers. Recall that the "echo merger" is defined by the disappearance of a separate reflectivity maxima. In nearly every case where the updrafts failed to merge but one of the reflectivity maxima disappeared, a new reflectivity maximum developed within minutes in association with one of the updrafts. The echoes associated with cells often separated again, becoming clearly discrete. The period during which only one maxima was evident never lasted longer than ten minutes. This suggests that the use of reflectivity-based criteria for storm merger can be taken with some confidence to also indicate updraft merger if a minimum length of time, on the order of ten minutes, is included in the definition. That is, if a reflectivity maximum disappears only briefly in close proximity to another while both are contained with some

relatively high contour, but reappears after ten or fifteen minutes, an updraft merger has likely not occurred.

Acknowledgments.

The authors would like to thank the National Center for Atmospheric Research for providing the cloud model CM1. This work was funded by National Science Foundation grant NSF-AGS-0801035.

References

Bluestein, H. B. and M. L. Weisman, 2000: The interaction of numerically simulated supercells initiated along lines. *Mon. Wea. Rev.*, **128**, 3128–3149.

Finley, C. A., W. R. Cotton, and R. A. Pielke Sr, 2001: Numerical simulation of tornadogenesis in a high precipitation supercell. Part I: Storm evolution and transition into a bow echo. *J. Atmos. Sci.*, **58**, 1597–1629.

Jewett, B. F., R. W. Przybylinsky, and R. B. Wilhelmson, 2006: Numerical simulation of the 24 April, 2002 storm merger between a left moving storm and supercell. Preprints, *23rd Conference on Severe Local Storms*, St. Louis, MO, Amer. Meteor. Soc., P11.3.

Klemp, J. B., 1987: Dynamics of tornadic thunderstorms. *Ann. Rev. Fluid Mech.*, textbf19, 369–402.

Lee, B. D., B. F. Jewett, and R. B. Wilhelmson, 2006: The 19 April 1996 Illinois tornado outbreak. Part II: Cell mergers and associated tornado incidence. *Wea. Forecasting*, **21**, 449–464.

Orville, H. D., Y. H. Kuo, R. D. Farley, and C. S. Hwang, 1980: Numerical simulation of cloud interactions. *J. Rech. Atmos.*, **14**, 499–516.

Tao, W. K. and J. Simpson, 1989: A further study of cumulus interactions and mergers: Three-dimensional simulations with trajectory analyses. *J. Atmos. Sci.*, **46**, 2974–3004.

Turpeinen, O., 1982: Cloud interactions and merging on day 261 of GATE. *Mon. Wea. Rev.*, **110**, 1238–1254.

Weisman, M. L. and J. B. Klemp., 1982: The dependence of numerically simulated convective storms on vertical wind shear and buoyancy. *Mon. Wea. Rev.*, **110**, 504–520.

_____, 1984: The structure and classification of numerically simulated convective storms in directionally-varying wind shears. *Mon. Wea. Rev.*, **112**, 2479–2498.

Westcott, N, 1984: A historical perspective on cloud mergers. *Bull. Amer. Meteor. Soc.*, **65**, 219–226.

_____, 1994: Merging of convective clouds: Cloud initiation, bridging and subsequent growth. *Mon. Wea. Rev.*, **122**, 780–790.

Wurman, J., Y. Richardson, C. Alexander, S. Weygandt, and P. F. Zhang, 2007: Dual-Doppler and single-Doppler analysis of a tornadic storm undergoing mergers and repeated tornadogenesis. *Mon. Wea. Rev.*, **133**, 97–119.